ACS SENSORS

Article

Cite This: ACS Sens. 2019, 4, 456−463

pubs.acs.org/acssensors

Miniaturized pH Holographic Sensors for the Monitoring of *Lactobacillus casei* Shirota Growth in a Microfluidic Chip

Leon C. Z. Chan,*[,†,§] Gita Khalili Moghaddam,[†] Zhiping Wang,[§] and Christopher R. Lowe[†]

[§]Singapore Institute of Manufacturing Technology (SIMTech), A*STAR, 2 Fusionopolis Way, Innovis, Singapore 138634

[†]Department of Chemical Engineering and Biotechnology, University of Cambridge, Tennis Court Road, Cambridge CB2 1QT, United Kingdom

ABSTRACT: Bioreactors have been used both to develop new, and to improve bioprocess yields for, biopharmaceutical products. However, efforts to miniaturize bioreactors, in order to save costs and accelerate process development times, have been limited by the lack of on-site monitoring capabilities available at such scales. In this study, small volume (3 nL) nonconsumptive holographic sensors were integrated into a glass-PDMS microfluidic chip to monitor via a blue-shift in the resultant holographic replay wavelength, the change in pH during microbial growth of *Lactobacillus casei* (*L. casei*) Shirota. Within the optimal growth pH range of *L. casei*, the accuracy of the miniaturized pH sensors was comparable to that of a conventional pH meter. Conceivably, this approach could be extrapolated to an array of miniaturized holographic sensors sensitive to different analytes, and thereby paving the way for reliable, real-time, noninvasive monitoring of microorganisms in a nanobioreactor.

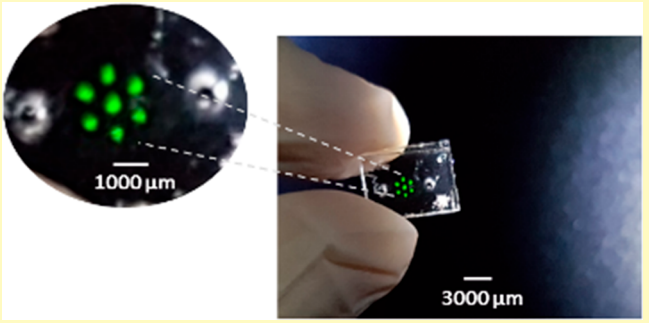

KEYWORDS: *holographic sensor, biosensor, pH monitoring, microfluidic chip, bacterial growth, microbioreactor, nanobioreactor*

Microfluidics is a technological field dealing with the precise transport of small (μL−pL) volumes of fluids.[1] The technology presents a suitable platform for the growth and monitoring of physiological parameters of small populations of living cells in microfluidic chambers (or bioreactors) in the micro- and nanoliter scale, also known as microbioreactors, and nanobioreactors, respectively. GlaxoSmithKline promoted the concept of microreactors in the late 1990s, and sought to have a microreactor pumping its product directly into a cell-based assay.[2]

The literature contains numerous examples of various microbioreactor systems, although very few have been commercialized.[3] Systems such as the Micro-Flask system (Applikon Biotechnology) and BioLector (m2p Laboratories) utilize microtiter plate format fermentation systems, while others such as Micro24 MicroReactor system (Pall Life Sciences) and ambr (Advanced Microscale Bioreactor System from The Automation Partnership) feature single-use bioreactors. The working volumes of these reactors range from 1 mL (BioLector)[3] and 7 mL (Micro24),[4] to 10−15 mL (ambr),[5] while SimCell (Seahorse Bioscience) microbioreactors have volumes ∼300−700 μL.[5] However, Zanzotto et al. revealed methods for *in situ* measurements of bioluminescence and fluorescence from bacterial cultures grown in 50 μL microbioreactors,[6] demonstrated 5−50 μL microbioreactors for real-time measurements in *Escherichia coli* cell culture and for global gene expression analysis.[7] The smallest microfluidic housing possible for the screen-printed electrode (SPE) fabricated by McKenzie et al. was 23 μL due to the SPE footprint and surface contours.[8] An approach to prevent biofilm formation enabled Balagaddé et al. to implement a miniaturized bioreactor with a working volume of 16 nL.[9]

The small absolute amount and low concentration of the cellular species of interest in microfluidic lab-on-chip devices present significant challenges for detection.[10] Furthermore, with substantial volume reductions compared to conventional bioreactors, the sampling time and minimum sampling volume is negatively impacted. For example, a typical 50 μL sample volume for high-performance liquid chromatography (HPLC) taken from a 100 mL bioreactor requires 500 turnovers of the chip volume, for which if the bacterial growth rate was 1 h^{-1}, a single sample can take 500 h,[11] which limits readings only to end-point measurements. Real-time monitoring of micro- and nanobioreactors with off-chip measurement techniques such as mid-infrared and Raman spectroscopy is thus not feasible.

Important physiological parameters such as pH, dissolved oxygen, carbon dioxide, and glucose have been monitored in a bioreactor. The sensor must be able to detect small concentration changes within a small volume in the nanobioreactor without significantly consuming the analyte. Traditional sensing techniques include electrochemical methods such as amperometry,[12−14] cyclic voltammetry,[15] and field-

Received: November 25, 2018
Accepted: January 15, 2019
Published: January 15, 2019

DOI: 10.1021/acssensors.8b01470
ACS Sens. 2019, 4, 456−463

effect transistors,[14,16] as well as chemical methods using phenol red[17,18] and fluorescent dyes,[19] fluorescence intensity,[20] and phase modulation lifetime fluorimetry.[14] However, these methods typically consume the analyte and affect or change the extracellular environment during measurements.

White light reflection holographic sensors are nonconsumptive, equilibrative sensors (refer to Figure 1b), which can be utilized to monitor bioreactor analytes in a label-free and noninvasive manner. Holographic sensors consist of holographic gratings embedded in an analyte-sensitive "smart hydrogel" which contains analyte-specific ligands (refer to Figure 1a). The gel matrix expands or contracts depending on the charge configuration of the ligands (Figure 1b), which results in a change in the Ag^0 nanoparticle interfringe distance, d (illustrated in Figure 1a), at different analyte concentrations. The embedded white light reflection (Denisyuk) hologram was fabricated by introducing an ordered multilayered arrangement of Ag^0 nanoparticles within the gel volume. This arrangement arises from the constructive interference of incident 532 nm laser during the holographic sensor fabrication process,[21] which is summarized as a process flow in Figure 1c.

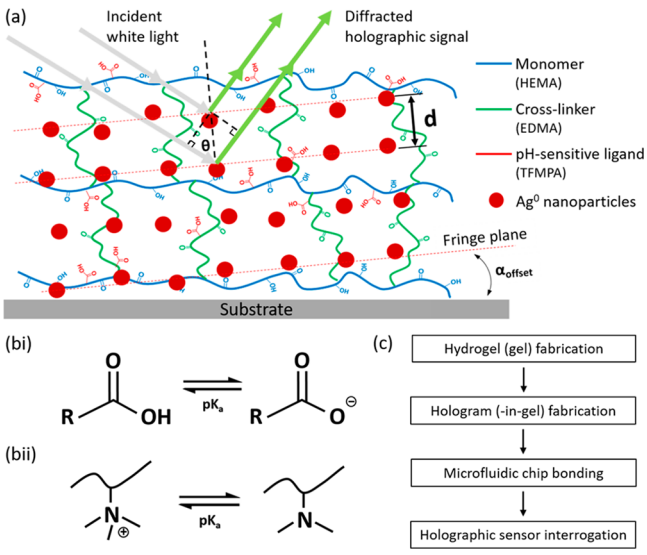

Figure 1. (a) Schematic diagram for holographic sensor pH-sensing concept. (b) Working principle for sensor−charge configuration of pH-sensitive ligand for (i) acidic moieties such as TMPA and (ii) basic moieties at low and high pH respectively. (c) Process flow for holographic sensor fabrication.

Any changes in gel volume will result in a corresponding shift in the fringe distance between each adjacent layer, due to Bragg's condition, eq 1, which in turn affects the resultant diffracted wavelength, or holographic signal, of incident white light.[21]

$$m\lambda = 2\eta d\cos\theta \quad (1)$$

where m is a positive integer, λ is the diffracted wavelength, η is the average gel refractive index, d is the distance between gratings, and θ is the incident angle to the normal.

Thus, imbibing water and counterions into the gel matrix during expansion, for example, when there is a net charge in the gel matrix, causes the mean fringe spacing between the Ag^0 nanoparticles, d, to increase. This increase in d translates to a red shift (colorimetric change) of the diffracted incident light.[22] Conversely, a contraction of the gel matrix results in a blue shift of the holographic signal.

In the pH-sensitive holographic sensor, acidic or basic methacrylate or acrylate moieties (illustrated in Figure 1b) were polymerized into the gel matrix to provide the protonateable/deprotonateable functionalities.

The pH-sensitive gel of the holographic sensor has been exploited to monitor the growth of bacterial cells such as *Lactobacillus casei* (*L. casei*).[23] *L. casei* is a homolactic fermentative bacterium, which produces lactic acid from carbohydrate substrates. As the cells multiply, the pH of the growth medium reduces with increasing cell density and thus the bacterial cell growth can be monitored by measuring the cell media pH in real time. The pH of the growth medium reduces from around pH 6.0 to pH 3.5 as the bacteria go through their exponential to stationary growth phase within 28 h of inoculation.

Lowe et al. (2004) hypothesized that 3 mm "spot" holographic sensors could be fabricated using a contact-printing process involving a hydrophobic FEP mask to inhibit polymerization at the masked regions where it was oxygen-rich.[24] In 2007, Dobson fabricated flake holograms under 1 μL in volume,[25] but only in suspensions or as random spots on a substrate. Bell (2011) utilized a tape mask to fabricate a spot holographic sensor of area about 1 cm^2 (10 μL, 11.3 mm diameter, 100 μm height) and incorporated it into a microfluidic chip to monitor the growth of *Lactobacillus casei*.[26] Although the pH sensor was utilized for the monitoring of *L. casei* in a microfluidic chip, the footprint (volume) of the sensor requires at least a > 11.3 mm microfluidic chamber diameter with >100 μm chamber height. The 20 min duration required for holographic signal equilibration was also not feasible for long-term real-time monitoring. In addition, although the sensor was nonconsumptive, it will still require a finite amount of analyte (H^+) to form the equilibrium, which in turn will alter its concentration in the extracellular environment. It is therefore imperative for the microfluidic chamber to possess a gel volume that minimizes the effect of the buffering capacity of the gel. The principal challenges for the miniaturization of the pH holographic sensor are thus miniaturizing the gel volume relative to the bioreactor volume and maximizing the holographic sensor signal.

By taking partial derivatives and summing for the total derivative of a cylindrical gel, a small change in the gel diameter has a 2× larger effect on volume (and hence its buffering capacity) than the same margin of change in gel height. It was calculated that with the reported 11.3 mm diameter (100 μm height) pH holographic sensor by Bell (2011),[26] a minimum 69.5 mm chamber diameter (350 μm chamber height to account for gel expansion) was required to safely neglect the gel buffering capacity. The sensor proposed in this study, 0.46 mm diameter (18.7 μm height), would require only a 1.69 mm chamber diameter (75 μm chamber height). The gel volume was determined by the rate of photopolymerization, which is influenced by UV intensity and uniformity, exposure duration, the concentration of monomers, cross-linkers, free radical initiator and inhibitor, and the degree of oxygen-isolation during photopolymerization. As the holographic replay signal is highly angular-specific, as expected from the Bragg's condition (eq 1), decreasing the holographic sensor diameter will require a corresponding increase in the holographic signal-to-noise ratio in order to detect a significantly attenuated signal from the miniaturized pH

DOI: 10.1021/acssensors.8b01470
ACS Sens. 2019, 4, 456−463

sensor. Furthermore, while a larger sensor is more tolerant to signal nonuniformity, since the wavelength of the holographic signal is integrated over a larger area, a miniaturized sensor will thus require being increasingly accurate and possessing a uniform holographic signal in order to minimize errors during sensor interrogation.

Out of the 400 nm visible range (380−780 nm) that a broadband white light source (380−780 nm) produces, only about 10 nm (from an ideal 10 nm full-width at half-maximum (fwhm) holographic signal) is diffracted by the Ag^0 gratings, while the rest passes through or is destructively impeded at a particular gel configuration. Furthermore, the available luminous flux from the incident light source was reduced drastically through the utilization of fiber optic cables (for light directionability and repeatability purposes) and source-to-sensor distance (due to space constraints). Assuming zero fiber transmission loss, 100% diffraction efficiency, 30% loss due to 10 cm fiber-to-sensor distance and 1:1 capture area to fiber diameter ratio, a Xenon light source coupled to a 0.6-mm-diameter fiber optic, together with the sensor diffractive selectivity of 10 nm out of the incident 400 nm range, would result in a 0.026% holographic signal flux. In other words, 99.974% of the incident light luminosity would be lost when reading the holographic signal. It was thus essential to maximize the diffraction efficiency and signal-to-noise ratio in order successfully to fabricate and detect a discernible signal.

For the resulting hologram to be useful as a sensor, the diffracted wavelength should have as narrow a full-width half-maximum (fwhm) signal as possible. This depends on the homogeneity of the polymerized gel, uniformity of the silver nanoparticles (Ag^0) within the gel matrix, and the regularity of diffraction gratings formed within the gel volume during the hologram fabrication process.

In this study, a miniaturized pH holographic sensor was fabricated by combining previous work by Bell (2011)[26] with photolithography (similar to Park et al. (2014)[27]) to produce the pH-sensitive "smart" gel. An offset method was devised and adapted from previous protocols by Leith and Upatnieks (1962)[28] and Marshall et al. (2003)[21] to produce high signal-to-noise volume reflection holograms within the gel matrix. This sensor was formed on a silanized glass substrate and bonded with polydimethylsiloxane (PDMS) bearing microchannel features to form a microfluidic chip for *L. casei* monitoring.

EXPERIMENTAL SECTION

Materials. 2-Hydroxyethyl methacrylate (HEMA), ethylene glycol dimethacrylate (EDMA), 2-(trifluoromethyl) acrylic acid (TFMPA), hydroquinone (HQ), and silver perchlorate anhydrous ($AgClO_4$) were supplied by Merck Ltd. 2-2-Dimethoxy-2-phenylacetophenone (DMPA) was purchased from Acros Organics. 4-Methylaminophenol sulfate (Metol) was procured from Aik Moh and L-ascorbic acid was obtained from Kanto Kagaku Singapore. Lithium bromide anhydrous was purchased from VWR Singapore.

The quartz-chrome photomasks and film photomasks were supplied by Front Range Photomask, USA and Infinite Graphics Pte Ltd., Singapore, respectively. The silicone and poly(methyl methacrylate) (PMMA) spacers were laser-cut, and the cyclic olefin copolymer (COC) covers were injection-molded and diced in-house.

The optomechanical apparatus for hologram fabrication was purchased from Acexon Technologies Pte Ltd., Singapore, while the optomechanical components of the customized holographic sensor interrogation setup were procured from CRS Engineering Pte Ltd., Singapore. The pH and conductivity meters were obtained from Mettler Toledo, the monochromator from PhotoniTech Pte Ltd., Singapore, the Avaspec spectrophotometer from Knight Photonics, UK, the high-resolution camera from iSolutions Technology Pte Ltd., and the white light interferometric 3D surface profiler from Bruker Singapore Pte Ltd.

Methodology. A pH holographic sensor consists of a white light reflection (Denisyuk) hologram recorded within the volume of a pH-sensitive hydrogel ("smart hydrogel"). A gel precursor solution comprising a monomer (HEMA), cross-linker (EDMA), solvent (IPA), pH-sensitive moiety (TFMPA), photoinitiator (DMPA), and polymerization inhibitor (HQ) was introduced between a 0.60-mm-thickness (8 mm × 8 mm) diced injection molded COC (cyclic olefin copolymer) and a scriber-cut silanized glass slide (12.5 mm × 9.4 mm). It was exposed to parallel-beam UV @ 29.64 mW/cm^2 for 4 min through a chrome-glass photomask with designated UV-transparent regions. The purpose of the COC cover was to exclude oxygen and minimize solvent evaporation during the photopolymerization process. For this work, 0.4-mm-diameter HEMA-*co*-TFMPA based hydrogel (gel) spots and arrays were UV-polymerized on a silanized glass slide.

Acetate film and glass-chrome photomasks with various transparent diameters ranging from 0.4 mm to 3 mm were utilized for selective photopolymerization. This technique, however, was not sufficient to produce well-defined and replicable hydrogel (gel) patterns on the silanized glass slide. A photoinhibitor, hydroquinone, was added to the gel precursor solution to quickly oxidize in the presence of UV and act as polymerization quenchers outside of the UV-illuminated region. The inhibitor thus limits photopolymerization by quenching any UV-initiated free radicals that diffuse out of the UV-illuminated region.

The photomask technique typically involves a highly collimated UV beam and intimate contact between the photomask and sample with semipolymerized (or semisolidified) for maximum mask fidelity. However, since the gel precursor solution is liquid, intimate contact is not possible and polymerization will produce widely variable gel heights.

Thick (0.25 mm) silicone films were utilized as uniform spacers and the setup placed on a nonreflective film photomask to minimize UV back-reflection. The UV source was placed as close as possible to the top photomask for optimal mask fidelity. The schematic diagram for the hydrogel (gel) fabrication setup and a typical photopolymerized gel were illustrated in Figure 3ai and Figure 3aii, respectively.

The gel precursor solution was introduced between the sample substrate and the COC cover. After UV photopolymerization, the substrate was rinsed thoroughly with isopropyl alcohol (IPA) and was immersed in 70% (v/v) ethanol for 12 min to dissolve unreacted constituents of the gel precursor solution. It also ensured that the gel would not delaminate from the glass substrate during the fabrication process.

The holograms were fabricated by diffusing silver perchlorate and lithium bromide into the gel matrix, exposure to a 532 nm laser (utilizing the hologram fabrication setup and substrate placement illustrated in Figure 2 and Figure 3bi), followed by development and fixing[21,23] and were scrutinized and modified to maximize signal-to-noise ratio. A glass cover was added to minimize evaporation and movement, and a front surface mirror utilized to minimize wavefront variation during hologram recording. An optimal substrate offset

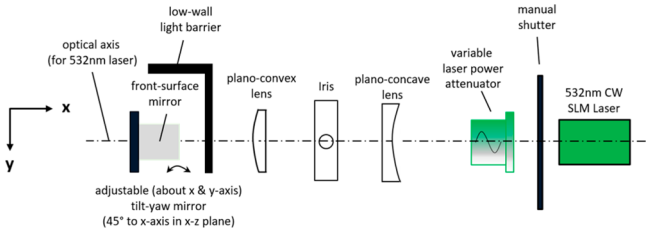

Figure 2. Schematic diagram of hologram fabrication setup.

DOI: 10.1021/acssensors.8b01470
ACS Sens. 2019, 4, 456−463

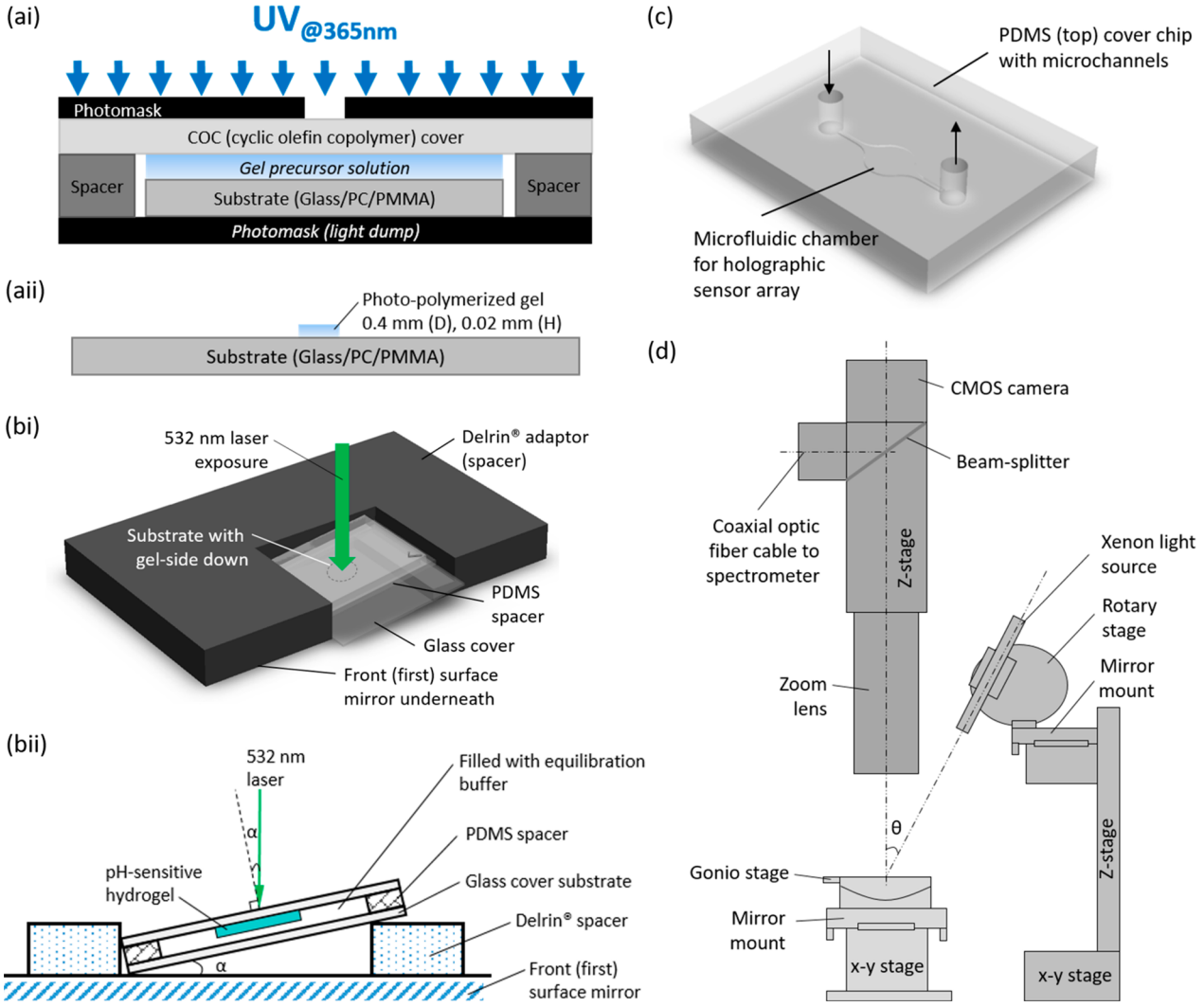

Figure 3. (ai) Schematic diagram for hydrogel (gel) fabrication. (aii) Illustration of photopolymerized gel after UV exposure. (b) 3D (i) and cross-sectional (ii) schematic diagram for substrate placement during (532 nm laser exposure) hologram fabrication. (c) Illustration of PDMS cover chip to be bonded to substrate (with photopolymerized gel) for PDMS-glass microfluidic chip fabrication.

angle, α of 7.16° (illustrated in Figure 3bii) was deduced from applying Snell's law at every interface to introduce a (resultant α_{offset} = 5°) Ag^0 fringe angle within the gel matrix (as depicted in Figure 1a). The small offset angle, α, was necessary to separate the reflected incident light (off the substrate surface) from the diffracted holographic signal. The holographic sensor was then enclosed in a microfluidic chip by bonding the substrate (where the gel was photopolymerized on) with a poly(dimethylsilxone) (PDMS) cover chip with microchannels (illustrated in Figure 3c) formed by soft lithography on a nickel mold produced using photolithography.

Due to the selective diffraction of incident light as it interacts with the Ag^0 fringe layers via constructive interference, there is only a small (narrow) angular window to observe the diffracted holographic signal. Consequently, a customized setup was designed, as described in Figure 3d, to interrogate the sensor signal. White light from a Xenon light source was transmitted via a fiber optic cable onto the gonio stage (where the sensor is placed) at a resultant angle, θ. This was so that only the diffracted holographic signal was picked up simultaneously (via a broadband beam splitter) by the CMOS camera and spectrometer (via a coaxial optic fiber cable). The customized holographic sensor interrogation setup allowed for 5 degrees of freedom (DOF) on the platform where the sensor was placed and 6 DOF on the jig where the light source was attached. This allowed for optimal capture of the diffracted holographic signal with narrow angular window.

To utilize the sensor as a predictive tool for pH measurement, the calibration curve equation (eq 4) was derived using the Henderson–Hasselbalch equation for acidic moieties (eq 2 and eq 3). It was based on the assumption that the working range of the sensor included the entire buffering capacity of the TFMPA pH moiety, coinciding with λ_{min} and λ_{max}, the sensor's most contracted and expanded configuration, respectively. Equation 5 was the derivative (and slope) of the predicted wavelength, λ. To obtain the predicted pH, eq 4 was rearranged to form eq 6.

$$\mathrm{pH} = \mathrm{p}K_a + \log_{10}\frac{[\mathrm{A}^-]}{[\mathrm{HA}]} \tag{2}$$

$$\alpha = \frac{[\mathrm{A}^-]}{[\mathrm{HA}] + [\mathrm{A}^-]} = \frac{\lambda - \lambda_{min}}{\lambda_{max} - \lambda_{min}} \tag{3}$$

$$\lambda = \frac{\lambda_{max}\cdot(10^{\mathrm{pH}-\mathrm{p}K_a}) + \lambda_{min}}{1 + 10^{\mathrm{pH}-\mathrm{p}K_a}} \tag{4}$$

$$\frac{\mathrm{d}\lambda}{\mathrm{d}\,\mathrm{pH}} = \frac{(10^{\mathrm{pH}-\mathrm{p}K_a}\cdot\ln 10)(\lambda_{max} - \lambda_{min})}{(1 + 10^{\mathrm{pH}-\mathrm{p}K_a})^2} \tag{5}$$

$$\mathrm{pH} = \log_{10}\left(\frac{\lambda - \lambda_{min}}{\lambda_{max} - \lambda}\right) + \mathrm{p}K_a \tag{6}$$

DOI: 10.1021/acssensors.8b01470
ACS Sens. 2019, 4, 456–463

Lactobacillus casei (*L. casei*) Shirota was chosen as the model organism for the pH sensor study, since it produces two lactic acid molecules from every glucose molecule.[29] Culturing *L. casei* in MRS (de Man, Rogosa and Sharpe) broth results in a reduction of pH and an increase in optical density at 600 nm (OD_{600}) to a maximum ~8.0 after 28 h. The broth pH typically commences at pH 6.0, and reduces to approximately pH 3.8 ~28 h after inoculating 1 cfu of *L. casei* into 70 mL of sterile MRS broth. The overnight inoculated broth was divided into 8−10 mL aliquots for hourly measurements from t = 14 h onward. The pH and OD_{600} were measured with a pH meter and a customized spectrophotometer with monochromator and cuvette holder, respectively. Conductivity was also measured with a conductivity meter.

RESULTS AND DISCUSSION

HEMA-*co*-TFMPA pH Holographic Sensor Spot. A 0.4-mm-diameter HEMA-*co*-TFMPA gel was fabricated using a glass-chrome photomask with a transparent window of the same diameter under parallel-beam UV illumination at low UV intensity (29.64 mW/cm^2). At higher UV intensities, the polymerized gel forms a ring instead of a cylindrical profile. The utilization of a photoinhibitor, hydroquinone, in the gel precursor solution and irradiation with a parallel UV beam were found to be essential for fabricating a consistent gel profile.

The resulting three-dimensional (3D) digital elevation model of the miniaturized pH holographic sensor (refer to Figure 4a) was obtained with the white light profiler. A 36×

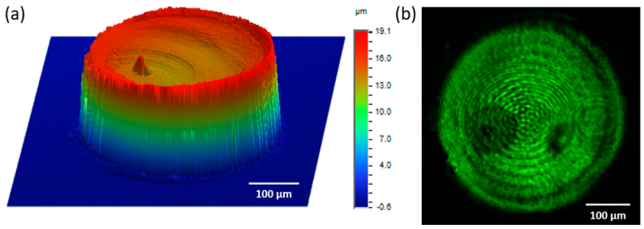

Figure 4. 0.4 mm HEMA-*co*-TFMPA sensor: (a) 3D digital elevation model of the 0.4 mm sensor after hologram fabrication. (b) Picture of the hologram taken by the high-resolution CMOS camera at 36× magnification while the 0.4 mm microfluidic chip embedded sensor was immersed in pH 6.0 McIlvaine buffer.

magnified picture of the holographic sensor spot was captured by the CMOS camera at angle θ from the illuminating light source (as depicted in Figure 3d), illustrated in Figure 4b.

The exposure time of the high-resolution camera was maintained constant at a value where the background (without the holographic signal) was dark. In addition, the integration time of the spectrometer was adjusted such that the highest signal intensity did not saturate and prevent accurate discrimination of peak wavelength.

To decouple the effect of ionic strength on the pH sensor, the prepared McIlvaine pH buffers utilized for sensor calibration were normalized to an ionic strength of 9.50 mS/cm. Other than measuring the wavelength response from the holographic sensor at pH 6.0, the average peak readings of three experimental runs (with ±1 s.d. error bars) at 0.25 pH unit intervals from pH 6.00 to pH 3.00 were calculated to plot the calibration curve for the HEMA-*co*-TFMPA pH sensor, as shown in Figure 5a. The apparent pK_a, λ_{min}, and λ_{max} were varied (based on eq 4) for the best-fit to the experimental data points. This apparent pK_a (pH 4.25) differed from the native

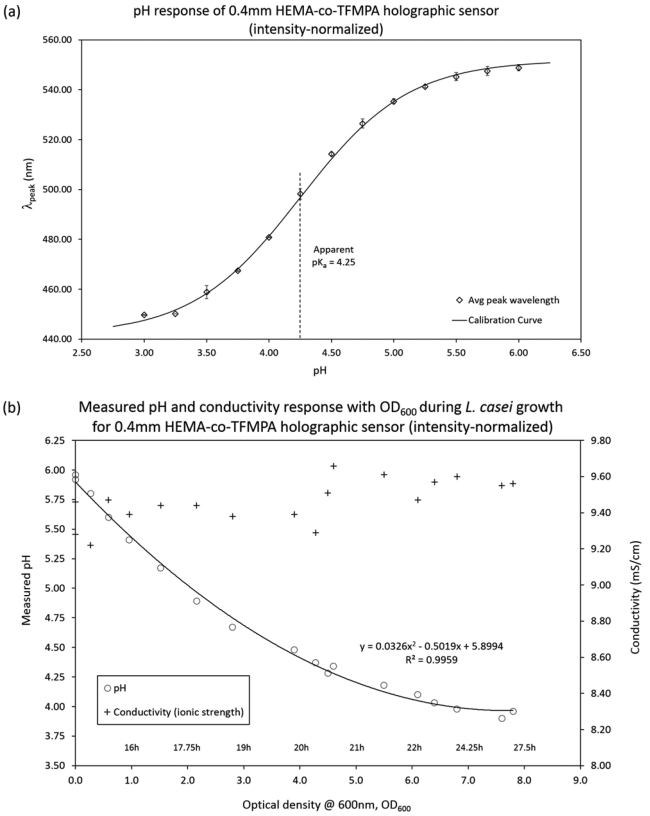

Figure 5. (a) Modified Henderson−Hasselbalch (H−H) pH calibration curve with the average of 3 runs (from pH 6.00 to pH 3.00), and error bars with ±1 s.d. The apparent pK_a is pH 4.25. (b) Measured pH and conductivity (ionic strength) of the batch media (broth) containing live *L. casei* from inoculation duration t = 14.00 h to t = 28.00 h at increasing OD_{600} values.

pK_a of the acidic TFMPA moiety by itself (pH 3.00) due to the influence of their polymeric microenvironment.[21]

In order to compare the holographic sensor accuracy, temperature-compensated pH, ionic strength, and optical density samples were measured at the same time as 50 μL *L. casei* from the same batch were introduced into the sensor-containing glass-PDMS microfluidic chip. Figure 5b illustrates these measured values on a graph with a best-fit curve. The observed random variations of ionic strength were within ±0.20 mS/cm throughout their inoculation duration, which even when taking into account the variation in ionic strength of the sensor, showed insignificant predicted pH differences. Taking into account ionic strength variation and the different (Xenon) light intensities at various wavelengths), the wavelength spectra of the sensor (diffracted holographic signal) read by the spectrometer from 13.5 to 26.0 h of *L. casei* inoculation (illustrated) were normalized and plotted in Figure 6a. At the same time, the CMOS camera captured the blue shift (caused by gel contraction) of the holographic sensor as the *L. casei* inoculation duration increased, pictured in Figure 6b. The average RGB values were captured from these images and transformed to the *xy*Y color space where the *x*-*y* values were plotted on the CIE 1931 chromaticity diagram. Figure 6c illustrates the locus traced out by the *x*-*y* values on the chromaticity diagram.

Since the pH of the samples of *L. casei* containing media was measured by a pH meter before being introduced into the microfluidic chip for sensor interrogation, the measured pH

DOI: 10.1021/acssensors.8b01470
ACS Sens. 2019, 4, 456−463

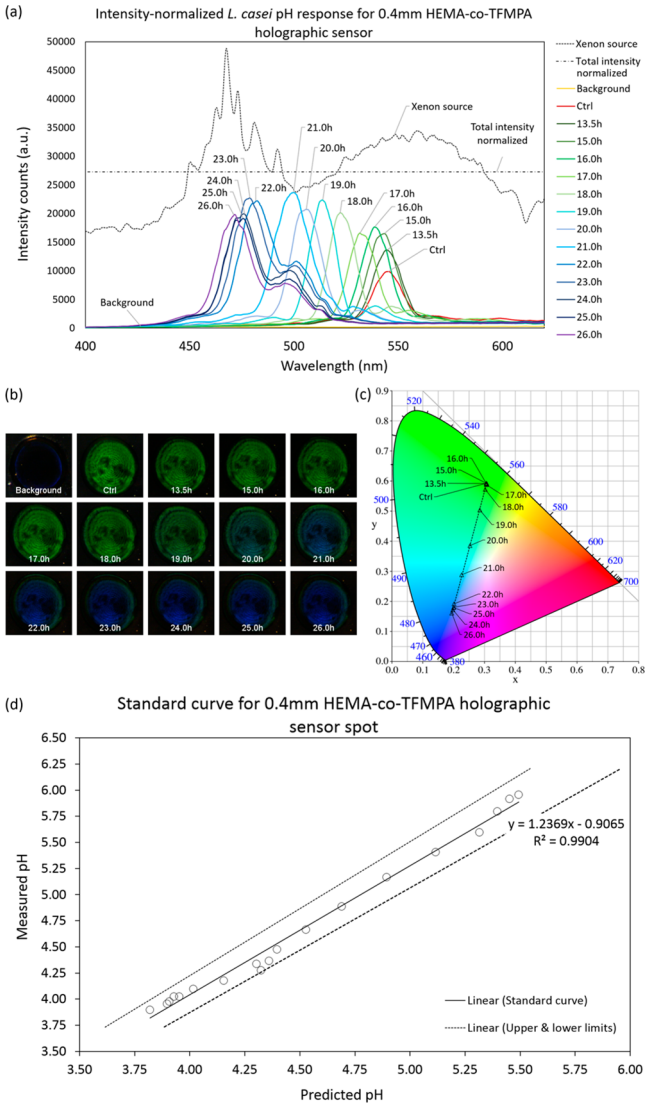

Figure 6. 0.4 mm HEMA-*co*-TFMPA holographic sensor response to *L. casei* growth: (a) Total intensity-normalized peak wavelength pH response obtained from batch (*L. casei*) process interrogation from t = 13.50 h to t = 26.00 h. The spectral response from the sensor was corrected with the total intensity normalized function of the Xenon light source at each data point across the observed visible spectrum (400–650 nm). (b) Picture montage of holograms taken with the high-resolution camera at 36× magnification corresponding to the batch sample introduced into the microfluidic chip at corresponding inoculation durations from t = 13.50 h to t = 26.00 h. (c) Visualization of color change with locus of the sensor response at corresponding *L. casei* inoculation durations from t = 13.50 h to t = 26.00 h. RGB-*xy*Y transformed values from (b) were plotted onto the CIE 1931 chromaticity diagram. (d) Standard curve for 0.4 mm HEMA-*co*-TFMPA holographic sensor illustrating the correlation between the measured and predicted pH.

can be compared with the predicted pH (acquired from eq 6) to visualize their respective relationship. As shown in Figure 6d, the upper and lower limits were determined by the zero point of the pH meter at pH 7.00 ± 0.25 (±3.57% allowable uncertainty), which was assigned throughout the pH measurement range to provide a visual boundary for the variability and accuracy of the predicted pH value. In other words, as long as the values stayed within the circumscribed region, the predicted pH values were as accurate as those measured with a conventional pH meter.

HEMA-*co*-TFMPA pH Holographic Sensor Array. In order to explore the manufacturing feasibility and replicability for multiple pH holographic sensors, a 7-spot holographic array was fabricated. Figure 7a illustrated the 3D digital elevation

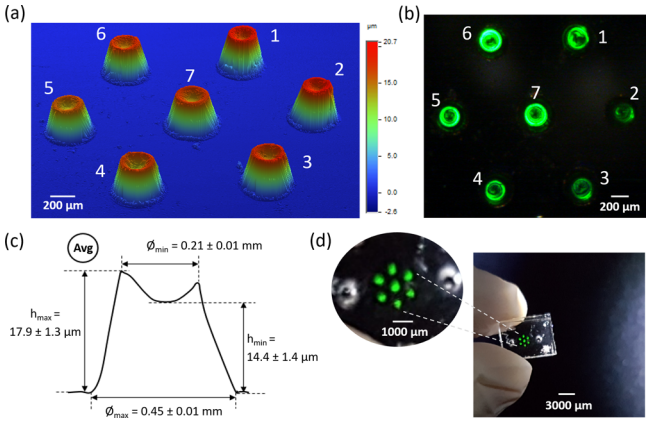

Figure 7. (a) 3D digital elevation model of the 0.4 mm holographic sensor array after hologram fabrication. (b) Picture of the hologram taken by the high-resolution camera at 6.96× magnification while the 0.4 mm microfluidic chip-embedded sensor array was immersed in pH 6.0 McIlvaine buffer. (c) Average (mean) dimensional profiles (with standard deviation) of the seven 0.4 mm sensors in the array. (d) Picture of the hologram array taken with a Samsung S7 mobile phone with pH 6.0 McIlvaine buffer inside the microfluidic chip.

model of the pH holographic sensor array. At angle θ from the axis of illumination (refer to Figure 3d), the holographic signal from the array was captured at 6.96× magnification (refer to Figure 7b). An indicative qualification of the sensor color can be determined using a mobile phone and LED torch depicted in Figure 7d. To achieve a coefficient of variation (CV) lower than 0.10 for each of the gel dimensional parameters (as described in Figure 7c), a combination of (i) parallel beam, (ii) narrow-band 365 nm UV LED, with (iii) a high-resolution glass-chrome photomask, and (iv) a high flatness cover substrate during photopolymerization were required.

At significantly higher UV intensities, the cross-sectional circular gel profile becomes increasingly ring-like.[27] Employing nonparallel (or multidirectional) UV or wavy cover substrates (W_q > 1.5 μm) can also lead to nondistinctive array patterns—gel polymerization will still occur at regions out of the UV-transparent region below the photomask. Depending on the quality of UV collimation and waviness of the cover substrate (which can act like a lens and change UV directionality), it has been found that the denser the array, the easier it was for nonspecific UV photopolymerization. This effect was further aggravated due to the low viscosity (~2 cP) of the gel precursor solution.

Aliquots of *L. casei* were extracted from ~15.25 h after bacterial inoculation to 28.00 h, and the holographic sensor response captured by the spectrometer and high-resolution camera. After obtaining a calibration curve for the sensor array with McIlvaine buffers, an intensity-normalized pH response together with the sensor peak wavelength profile was plotted in Figure 8a. The magnified picture of the array at different inoculation durations (corresponding to the pH decrease from the bacteria's metabolism of glucose to lactic acid) was shown

DOI: 10.1021/acssensors.8b01470
ACS Sens. 2019, 4, 456–463

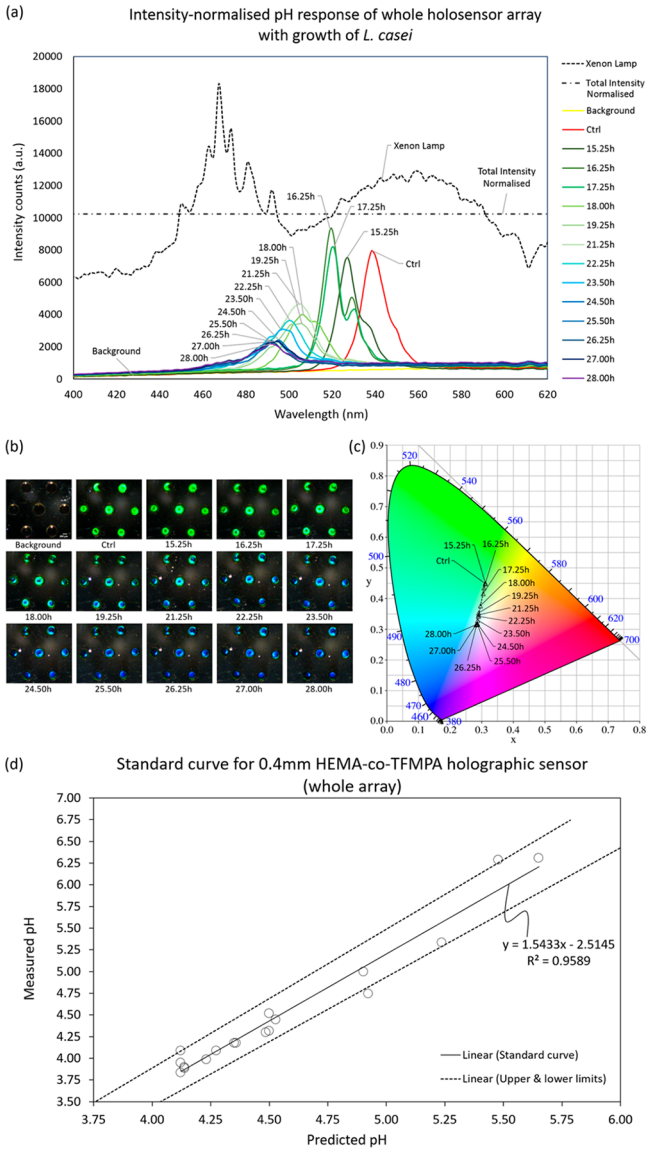

Figure 8. (a) Total intensity-normalized peak wavelength sensor array *L. casei* pH response obtained from batch process interrogation from t = 15.25 h to t = 28.00 h. (b) Montage of holograms taken with the high-resolution camera at 6.96× magnification corresponding to the batch sample introduced into the microfluidic chip at corresponding inoculation durations from t = 15.25 h to t = 28.00 h. (c) Visualization of the color change with locus of the sensor responses at corresponding inoculation durations from t = 15.25 h to t = 28.00 h. RGB-*xy*Y transformed values from (b) were plotted onto the CIE 1931 chromaticity diagram. (d) Standard curve for 0.4 mm HEMA-*co*-TFMPA sensor array illustrating the correlation between the measured and predicted pH. The data points within the upper and lower limits of the standard curve for the holographic sensor spot and array, as illustrated in Figure 6d and Figure 8d respectively, showed that the miniaturized pH holographic sensors were as accurate and reliable as a conventional pH meter in monitoring (pH reduction) *L. casei* growth in a PDMS-glass microfluidic chip.

in Figure 8b while the RGB-to-*xy*Y color space transformation obtained from the captured image of the array showed the color change on the CIE 1931 chromaticity diagram in Figure 8c.

Although separate readings for each spot were taken, the peak wavelength response for all seven spots in the array as a whole was utilized to average out the effects of individual spots.

The predicted pH from the holographic sensor array was determined using eq 6 and pK_a, λ_{min}, and λ_{max} values were obtained from the calibration curve of the sensor array. To ensure that the sensor can be utilized accurately for *L. casei* monitoring, a standard curve (Figure 8d) for the whole array was plotted with the measured pH against its predicted pH. The zero point error (assumed constant value of the reported ±3.57% throughout the measured pH range) of the pH meter was visually represented as the upper (+ 3.57%) and lower (−3.57%) limit.

CONCLUSIONS

Noninvasive optical techniques for sensor interrogation are preferred over electrochemical methods, as they do not require electrical connections or electrodes that are prone to biofouling and corrosion. It is also essential that the sensor does not consume the analyte it is measuring, especially when monitoring cells in a < 250 μL microfluidic chamber.

In this study, a miniaturized pH holographic sensor spot and array were fabricated in a glass-PDMS chip, which was utilized to monitor the decrease in pH from *L. casei* metabolism. The peak wavelength signal from the reflection hologram was obtained and the predicted pH calculated using equations derived from first-principles and a calibration curve for that particular sensor spot or array. The accuracy of the predicted pH was comparable to that of a standard pH meter. This enables pH readings to be measured optically and without consuming protons and thereby affecting the pH value of the culture medium in a microfluidic chamber.

This work will facilitate the realization of nonconsumptive sensing and monitoring of extracellular environments and can be further sensitized for single-cell monitoring. The miniaturized sensors are also suitable for integration into diagnostic, point-of-care, and wearable devices.

AUTHOR INFORMATION

Corresponding Author

*E-mail: czchan@SIMTech.a-star.edu.sg.

ORCID

Leon C. Z. Chan: 0000-0001-7712-1060

Author Contributions

The manuscript was written through contributions of all authors.

Notes

The authors declare no competing financial interest.

ACKNOWLEDGMENTS

The authors thank Dr. Colin A.B. Davidson and Dr. Jeffrey Blyth for valuable discussions on aspects related to this work. The research reported in this publication was supported with the A*STAR Graduate Scholarship (Overseas) (for LCZ Chan) by the Agency for Science, Technology and Research (A*STAR) Graduate Academy (A*GA), Singapore.

REFERENCES

(1) Zimmerman, W. B. J. *Microfluidics: History, Theory and Applications*; Zimmerman, W. B. J., Ed.; CISM International Centre for Mechanical Sciences; Springer Science & Business Media, 2006.

DOI: 10.1021/acssensors.8b01470
ACS Sens. 2019, 4, 456−463

(2) Hogan, J. Lab on a Chip: A Little Goes a Long Way. *Nature* **2006**, *442* (7101), 351−352.
(3) Rohe, P.; Venkanna, D.; Kleine, B.; Freudl, R.; Oldiges, M. An Automated Workflow for Enhancing Microbial Bioprocess Optimization on a Novel Microbioreactor Platform. *Microb. Cell Fact.* **2012**, *11* (144), 1−13.
(4) Pörtner, R. *Animal Cell Biotechnology: Methods and Protocols*, 3rd ed.; Pörtner, R., Ed.; Methods in Molecular Biology; Humana Press, 2014.
(5) Bareither, R.; Pollard, D. A Review of Advanced Small-Scale Parallel Bioreactor Technology for Accelerated Process Development: Current State and Future Need. *Biotechnol. Prog.* **2011**, *27* (1), 2−14.
(6) Zanzotto, A.; Boccazzi, P.; Gorret, N.; Van Dyk, T. K.; Sinskey, A. J.; Jensen, K. F. In Situ Measurement of Bioluminescence and Fluorescence in an Integrated Microbioreactor. *Biotechnol. Bioeng.* **2006**, *93* (1), 40−47.
(7) Zanzotto, A.; Szita, N.; Boccazzi, P.; Lessard, P.; Sinskey, A. J.; Jensen, K. F. Membrane-Aerated Microbioreactor for High-Throughput Bioprocessing. *Biotechnol. Bioeng.* **2004**, *87* (2), 243−254.
(8) McKenzie, J. R.; Cognata, A.; Davis, A. N.; Wikswo, J. P.; Cliffel, D. E. Real-Time Monitoring of Cellular Bioenergetics with a Multi-Analyte Screen-Printed Electrode. *Anal. Chem.* **2015**, *87*, 7857−7864.
(9) Balagaddé, F. K.; You, L.; Hansen, C. L.; Arnold, F. H.; Quake, S. R. Long-Term Monitoring of Bacteria Undergoing Programmed Population Control in a Microchemostat. *Science (Washington, DC, U. S.)* **2005**, *309* (5731), 137−140.
(10) Sims, C. E.; Allbritton, N. L. Analysis of Single Mammalian Cells On-Chip. *Lab Chip* **2007**, *7* (4), 423−440.
(11) Lee, K. S.; Boccazzi, P.; Sinskey, A. J.; Ram, R. J. Microfluidic Chemostat and Turbidostat with Flow Rate, Oxygen, and Temperature Control for Dynamic Continuous Culture. *Lab Chip* **2011**, *11* (10), 1730−1739.
(12) Pasirayi, G.; Auger, V.; Scott, S. M.; Rahman, P. K. S. M.; Islam, M.; O'Hare, L.; Ali, Z. Microfluidic Bioreactors for Cell Culturing: A Review. *Micro Nanosyst.* **2011**, *3* (2), 137−160.
(13) Luo, X.; Davis, J. J. Electrical Biosensors and the Label Free Detection of Protein Disease Biomarkers. *Chem. Soc. Rev.* **2013**, *42* (13), 5944−5962.
(14) Herber, S.; Bomer, J.; Olthuis, W.; Bergveld, P.; van den Berg, A. A Miniaturized Carbon Dioxide Gas Sensor Based on Sensing of PH-Sensitive Hydrogel Swelling with a Pressure Sensor. *Biomed. Microdevices* **2005**, *7* (3), 197−204.
(15) Gracia, R.; Mecerreyes, D. Polymers with Redox Properties: Materials for Batteries, Biosensors and More. *Polym. Chem.* **2013**, *4* (7), 2206−2214.
(16) Zhang, Z.; Boccazzi, P.; Choi, H.-G.; Perozziello, G.; Sinskey, A. J.; Jensen, K. F. Microchemostat-Microbial Continuous Culture in a Polymer-Based, Instrumented Microbioreactor. *Lab Chip* **2006**, *6* (7), 906−913.
(17) Matteau, D.; Baby, V.; Pelletier, S.; Rodrigue, S. A Small-Volume, Low-Cost, and Versatile Continuous Culture Device. *PLoS One* **2015**, *10* (7), 1−13.
(18) Shaegh, S. A. M.; De Ferrari, F.; Zhang, Y. S.; Nabavinia, M.; Mohammad, N. B.; Ryan, J.; Pourmand, A.; Laukaitis, E.; Sadeghian, R. B.; Nadhman, A.; et al. A Microfluidic Optical Platform for Real-Time Monitoring of PH and Oxygen in Microfluidic Bioreactors and Organ-on-Chip Devices. *Biomicrofluidics* **2016**, *10* (4), No. 044111.
(19) Nayak, M.; Singh, D.; Singh, H.; Kant, R.; Gupta, A.; Pandey, S. S.; Mandal, S.; Ramanathan, G.; Bhattacharya, S. Integrated Sorting, Concentration and Real Time PCR Based Detection System for Sensitive Detection of Microorganisms. *Sci. Rep.* **2013**, *3* (3266), 1−7.
(20) Pickup, J. C.; Hussain, F.; Evans, N. D.; Rolinski, O. J.; Birch, D. J. S. Fluorescence-Based Glucose Sensors. *Biosens. Bioelectron.* **2005**, *20* (12), 2555−2565.
(21) Marshall, A. J.; Blyth, J.; Davidson, C. A. B.; Lowe, C. R. PH-Sensitive Holographic Sensors. *Anal. Chem.* **2003**, *75* (17), 4423−4431.
(22) Marshall, A. J.; Kabilan, S.; Blyth, J.; Lowe, C. R. Analyte-Responsive Holograms for (Bio)Chemical Analysis. *J. Phys.: Condens. Matter* **2006**, *18* (18), S619−S626.
(23) Bell, L. L.; Seshia, A. A.; Davidson, C. A. B.; Lowe, C. R. Integration of Holographic Sensors into Microfluidics for the Real-Time PH Sensing of L. Casei Metabolism. *Procedia Eng.* **2010**, *5*, 1352−1355.
(24) Lowe, C. R.; Davidson, C. A. B.; Blyth, J.; Marshall, A. J.; James, A. P. Holographic Sensors and Their Production; International Patent WO 2004081546A1, 2004.
(25) Dobson, C. A. The Design, Fabrication and Characterization of Holographic Optical Elements; PhD Thesis; University of Cambridge, 2007.
(26) Bell, L. L. Optically Interrogated Biosensors in Microfluidics; PhD Thesis; University of Cambridge, 2011.
(27) Park, S.; Kim, D.; Ko, S. Y.; Park, J.-O.; Akella, S.; Xu, B.; Zhang, Y.; Fraden, S. Controlling Uniformity of Photopolymerized Microscopic Hydrogels. *Lab Chip* **2014**, *14*, 1551−1563.
(28) Leith, E. N.; Upatnieks, J. Reconstructed Wavefronts and Communication Theory. *J. Opt. Soc. Am.* **1962**, *52* (10), 1123−1130.
(29) Gaynor, P. Generally Recognized as Safe (GRAS) Determination for the Use of Lactobacillus Casei Strain Shirota As a Food Ingredient, 2012.

DOI: 10.1021/acssensors.8b01470
ACS Sens. 2019, 4, 456−463